CHEMISTRY
A EUROPEAN JOURNAL

DOI: 10.1002/chem.201103445

Construction of a Graphene Oxide Based Noncovalent Multiple Nanosupramolecular Assembly as a Scaffold for Drug Delivery

Yang Yang,[a] Ying-Ming Zhang,[a] Yong Chen,[a] Di Zhao,[a] Jia-Tong Chen,[b] and Yu Liu*[a]

Abstract: A multiple supramolecular assembly, in which a folic acid-modified β-cyclodextrin (**1**) acted as a target unit, an adamantanyl porphyrin (**2**) acted as a linker unit, and graphene oxide acted as a carrier unit, was successfully fabricated through non-covalent interactions and comprehensively investigated by means of UV/Vis, fluorescence, and X-ray photoelectron spectroscopies, and electron microscopy. Significantly, the graphene oxide unit could associate with the anticancer drug doxorubicin through π–π interactions, and the folic acid-modified β-cyclodextrin unit could recognize the folic acid receptors in cancer cells. Owing to the cooperative contribution of these three units, the resulting multiple supramolecular assembly, after association with doxorubicin, exhibited better drug activity and much lower toxicity than free doxorubicin in vivo.

Keywords: cyclodextrins · folic acid · self-assembly · supramolecular chemistry · targeted delivery

Introduction

Structurally well-organized nanoarchitectures with biocompatible and optoelectronic functionalities based on the control of weak bonding interactions provide critical insight into the topic of bottom-up molecular manipulation. In particular, bioactive nanosupramolecules constructed from multifunctional components through noncovalent driving forces, such as liposomes,[1] inorganic nanoparticles,[2] polymeric micelles,[3] and carbon nanomaterials,[4] have found applications in delivering therapeutic drugs and diagnostic agents into tumors at the cellular and in vivo levels, mainly due to their advantages of controllable release, on-demand delivery, and enhanced therapeutic efficacy in cells and tissues. Compared with traditional drug-delivery systems that have little or no specificity, supramolecular biotechnology demonstrates the power to remarkably increase the bioavailability of clinically relevant drugs at active sites and avoid multidrug resistance to a great extent.[5] Graphene oxide (GO), a "rising star" material with a thickness of one atom and a large two-dimensional structure,[6] can strongly bind with various organic or biological molecules through chemical modifications and thus promote practical innovations in biological systems, such as nanometer-sized carriers of drugs and genes. GO is also much more efficacious than other carbonaceous nanomaterials by virtue of its large specific surface area and extended π-conjugated system.[7] For instance, Dai and coworkers have reported single-walled carbon nanotubes and GO modified with polyethylene glycol, targeted agents, and chemotherapeutic drugs through non-covalent interactions, and implemented specific cell-killing and antitumor activity in living systems.[4,8] Moreover, the cytotoxicity of two anticancer drugs on the surface of functionalized nanoscale GO was significantly higher than a single drug on GO in cancer cells, which highlights the enhanced therapeutic efficacy and potential clinical advantages of graphene-based nanocarriers.[9]

Herein, a molecular-recognition strategy and noncovalent nanotechnology were used to construct an integrated multifunctional system by a supramolecular surface modification of GO with folic acid (FA) through a synthetic bifunctional molecule that contains a planar porphyrin moiety as a binding group and an adamantane moiety that is encapsulated in the cavity of cyclodextrin. By taking advantage of the mutual cooperation of FA-modified β-cyclodextrin **1** (FA-CD), adamantane-grafted porphyrin **2**, and GO, the structural integrity of GO was preserved and the resultant supramolecular assemblies could specifically carry doxorubicin (DOX) into folate-receptor-positive malignant cells without imparting an enhanced toxicity (Scheme 1).

[a] Y. Yang, Dr. Y.-M. Zhang, Prof. Dr. Y. Chen, D. Zhao, Prof. Dr. Y. Liu
Department of Chemistry
State Key Laboratory of Elemento-Organic Chemistry
Nankai University, Tianjin, 300071 (P. R. China)
Fax: (+86) 22-2350-3625
E-mail: yuliu@nankai.edu.cn

[b] J.-T. Chen
Department of Biochemistry and Molecular Biology
College of Life Sciences
Nankai University, Tianjin, 300071 (P. R. China)

Supporting information for this article is available on the WWW under http://dx.doi.org/10.1002/chem.201103445, and contains details of the synthetic routes and characterization of **1** and **2**, UV/V spectra of **2**/GO and DOX/GO, fluorescence spectra of **2**/GO and DOX/GO, FT-IR spectra and TGA curves of **2**/GO, DOX/GO, and DOX/**2**/GO, XPS C1s and N1s spectra of GO, **2**/GO, and DOX/**2**/GO, cytotoxicity experiment results over 48 h, and cure effect pictures of nude mice.

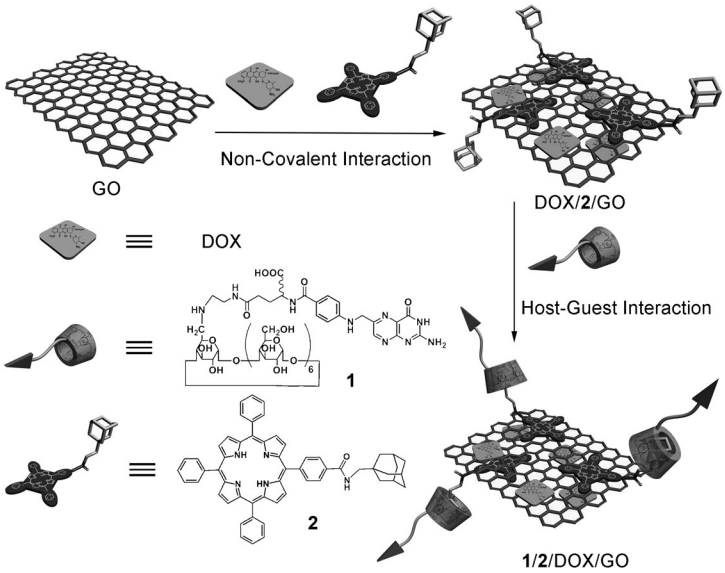

Scheme 1. Synthesis of **1**/**2**/DOX/GO from graphene oxide, DOX, adamantane-modified porphyrin, and folic acid modified cyclodextrin.

Results and Discussion

Synthesis: Compound **1** was synthesized in 31% yield by an amide condensation reaction between FA and mono-6-deoxy-6-ethylenediamino-β-CD, and was comprehensively characterized by ^{1}H and ^{13}C NMR spectroscopy, MALDI-MS, and elemental analysis (Schemes S1–S2 and Figures S1–S6 in the Supporting Information). The 2D ROESY spectrum of **1** in D_2O exhibited obvious NOE correlations between the interior protons of CD and the neopterin ring of FA, which suggests the formation of an intramolecular self-inclusion complex in **1** (Figure S7 in the Supporting Information). Due to the low solubility of **2** in water, sodium adamantane carboxylate was chosen as a reference to demonstrate the binding mode in the presence of an adamantanyl moiety. As shown in Figures 1 and S8 (in the Supporting Information), the introduction of the adamantane molecules drives the neopterin ring out of the CD cavity, which facilitates an intermolecular interaction between the FA moiety and folate-receptor-positive malignant cells.

Next, the nanosupramolecular assembly of DOX/**2**/GO was conveniently constructed through a π–π interaction between DOX, porphyrin, and GO. From a calculation of the binding constant between β-CD and adamantanecarboxylic acid[10] and the concentrations of host and guest molecules, about 7% of **2** in DOX/**2**/GO could be converted to a **1**/**2** complex under our experimental conditions. This surface coverage of DOX/**2**/GO by **1** is within the optimal cell transfection coverage of 5–9%.[11]

Spectroscopic and thermogravimetric studies: The photophysical behavior of DOX/**2**/GO was fully investigated by means of UV/Vis and fluorescence spectroscopy. In the UV/Vis spectrum of **2**/GO (Figure S9 in the Supporting Information) and DOX/**2**/GO (Figure 2) assemblies, the Soret and Q bands of the porphyrin unit showed large bathochromic shifts of around 18 and 13 nm, respectively, which indicates that the phenyl groups and the porphyrin ring of **2** adopted a more coplanar conformation to enhance the π conjugation and to firmly interact with GO.[12] Compared with the characteristic absorption of DOX at $\lambda = 490$ nm, the UV/Vis spectrum of DOX/GO (Figure S10 in the Supporting Information) showed a bathochromic shift of about 8 nm, which indicates complexation between DOX and GO.[8] The loading ratio (the weight ratio of loaded drug to carrier)[9] of DOX on the surface of GO was calculated to be 168% according to the photometric standard curve of DOX at $\lambda =$ 490 nm and GO at $\lambda = 680$ nm (Figure 3), which is consistent with the reported value of 150%.[9]

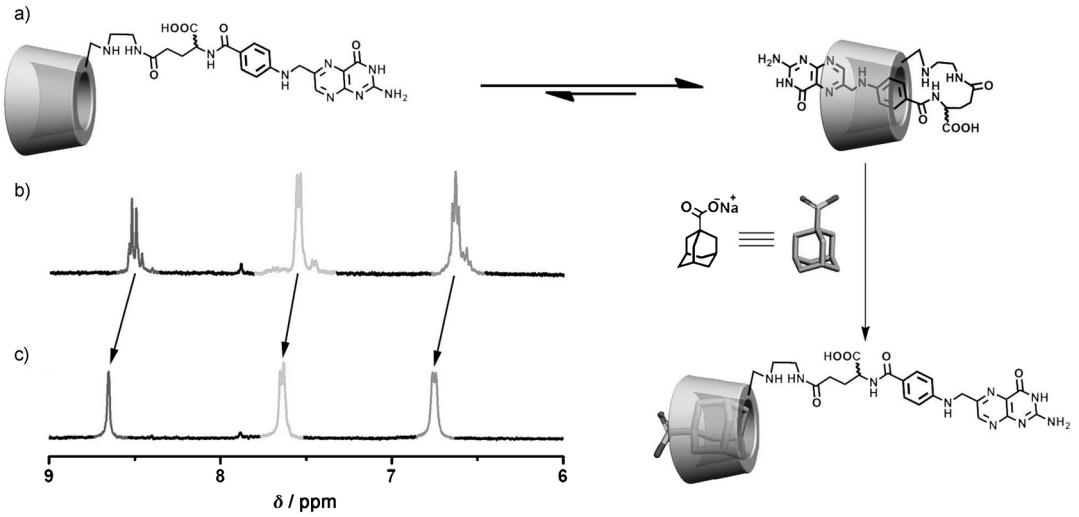

Figure 1. a) Schematic representation of the intermolecular interaction between **1** and the adamantanyl moiety. b) and c) Partial ^{1}H NMR spectral changes for the neopterin ring of **1** (5 mM) b) in the absence and c) in the presence of sodium adamantane carboxylate (83 mM) in D_2O at 25°C.

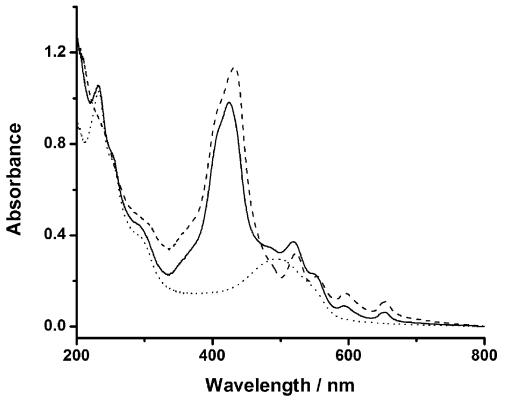

Figure 2. UV/Vis spectra of DOX/GO (•••••), **2**/GO (-----), and DOX/**2**/GO (——) in aqueous solution.

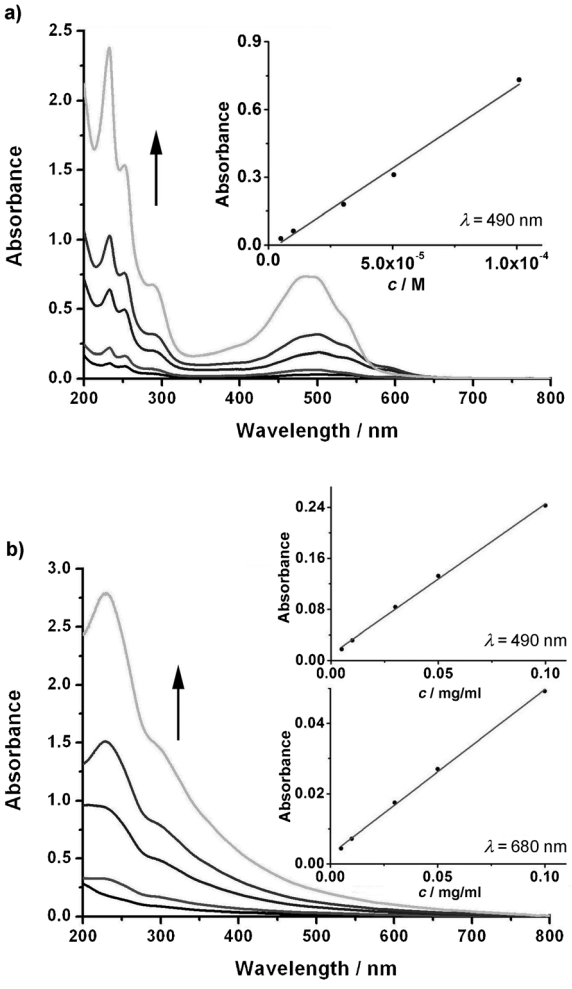

Figure 3. a) UV/Vis spectra of DOX at 5.05, 10.1, 30.3, 50.5, 101 μM. Inset: Standard curve of DOX with absorption at $\lambda = 490$ nm vs. concentration. b) UV/Vis spectra of GO at 0.005, 0.01, 0.03, 0.05, 0.10 mg mL^{-1}. Inset: Standard curve of GO with absorption at $\lambda = 490$ and 680 nm vs. concentration.

As illustrated in Figure S11 in the Supporting Information, the fluorescence intensity of DOX and **2** after loading onto GO was decreased by 93 and 97%, respectively, due to π–π stacking interactions that result in photoinduced electron and/or energy transfer to the acceptor graphene oxide.[12,13] FT-IR spectroscopy and thermogravimetric analysis (TGA) were also carried out to further characterize the DOX/**2**/GO assembly, and jointly demonstrated the multidimensional nanoarchitectures of **1**/**2**/DOX/GO (Figure S12–S13 in the Supporting Information).

X-ray photoelectron spectroscopy: As an effective technique for surface analysis, X-ray photoelectron spectroscopy (XPS) was performed to quantitatively determine the surface element composition in GO, **2**/GO, and DOX/**2**/GO.[14] As seen in Figure 4a and Figure S14 in the Supporting Information, the asymmetric C1s spectrum of GO can be typically assigned to three components (284.6, 286.9, and 288.6 eV).[15] The peak at 284.6 eV was attributed to sp^2-hybridized graphene carbon atoms and those bound to hydrogen atoms.[16] The peak at 286.9 eV was assigned to C–O, whereas the peak at 288.6 eV was assigned to C=O and COOH groups.[17] The C1s and N1s spectra of **2**/GO (Figure 4b and Figure S15–S16 in the Supporting Information) could also be divided into characteristic peaks of functional groups for each component, but were not simple mixtures of the peaks of GO and **2**. Furthermore, all the corresponding peaks of associated elements were observed in the XPS survey spectrum of DOX/**2**/GO, which confirmed the formation of supramolecular architecture (Figure 4c). That is, the C1s spectrum of DOX/**2**/GO consisted of four components (284.6, 286.3, 288.0, and 291.0 eV; Figure S17 in the Supporting Information). Besides the graphene carbon atoms at 284.6 eV, peaks at 286.3, 288.0, and 291.0 eV were assigned to C–O (C=N and C–NH), C=O (CO–NH and COOH), and an sp^2-hybridized carbon π*←π shake-up, respectively. The appearance of C=N, C–NH, and C–NH$_2$ at 286.3 eV and CO–NH at 288.0 eV also further indicate the successful loading of DOX and **2** onto GO. Additionally, the N1s spec-

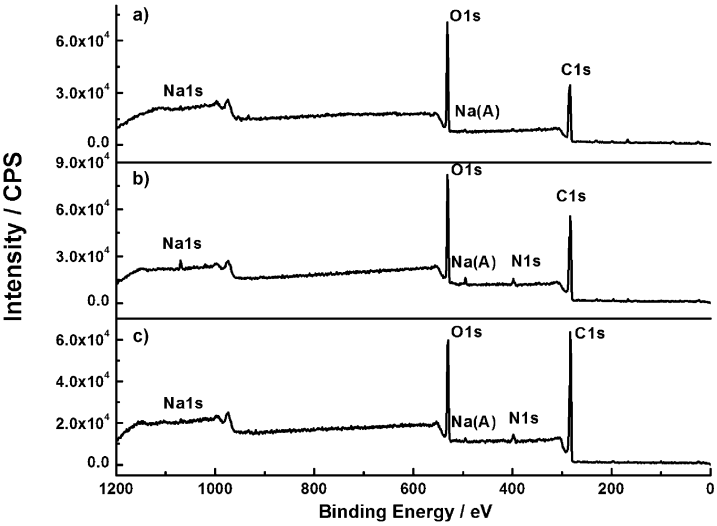

Figure 4. XPS spectra of a) GO, b) **2**/GO, and c) DOX/**2**/GO.

trum of DOX/**2**/GO was composed of three components, in which the peaks at 397.6, 399.6, and 401.7 eV were assigned to C=N, C−N, and CO−NH (C−NH_2), respectively (Figure S18 in the Supporting Information).[18] It should be noted that the sodium atoms were introduced as carboxylates on the surface of GO. The loading ratios of **2** and DOX in **2**/GO, DOX/GO, and DOX/**2**/GO systems were derived from the content ratio of C, O, and N atoms and are listed in Table S1 in the Supporting Information. The content change in these systems can be explained as follows. Due to the poor solubility in water, compound **2** may exist as a self-aggregate on the surface of GO; this was further confirmed by AFM images of **2**/GO (see below). If both **2** and DOX are loaded onto GO, the competition between DOX and **2** through π–π stacking could have potent inhibitory effects on the self-aggregation of porphyrins and thus decrease the content of DOX in DOX/**2**/GO assembly to some extent.

HR-TEM and AFM images: The morphology of DOX/**2**/GO assembly was directly obtained by high-resolution transmission electron microscopy (HR-TEM) and atomic force microscopy (AFM). As seen in the HR-TEM image (Figure 5a), the DOX/**2**/GO assembly showed a tendency to self-aggregate at a relatively high concentration (0.13 mg mL^{-1}), and the surface dimensions were measured to be around 400 to 500 nm.

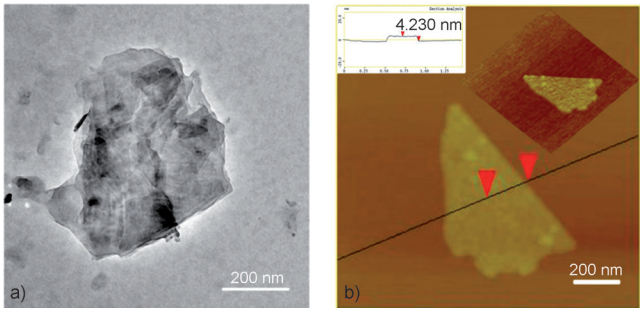

Figure 5. Typical a) TEM and b) AFM images of DOX/**2**/GO.

In a control experiment, the AFM images of free GO in a dilute solution showed a monodisperse sheet-like morphology with lateral dimensions ranging from hundreds of nanometers to micrometers and an average height of 0.8 to 1.0 nm (Figure 6a), assigned to totally exfoliated GO single layers. When loading **2** and/or DOX onto GO, repeated ultrasonication of the samples cracked the GO into sheets of 300 to 400 nm, which would be suitable for biological applications.[13] In addition, the AFM images of **2**/GO indicated that **2** was loaded onto GO as both monomers and molecular aggregates. Herein, the GO sheet zone functionalized by monomers of **2** showed an average height of 2.5 nm (Figure 6b), which is consistent with the sum of the height of the monolayer of GO, the π–π stacking distance, and the diameter of the adamantanyl group. In the AFM images of

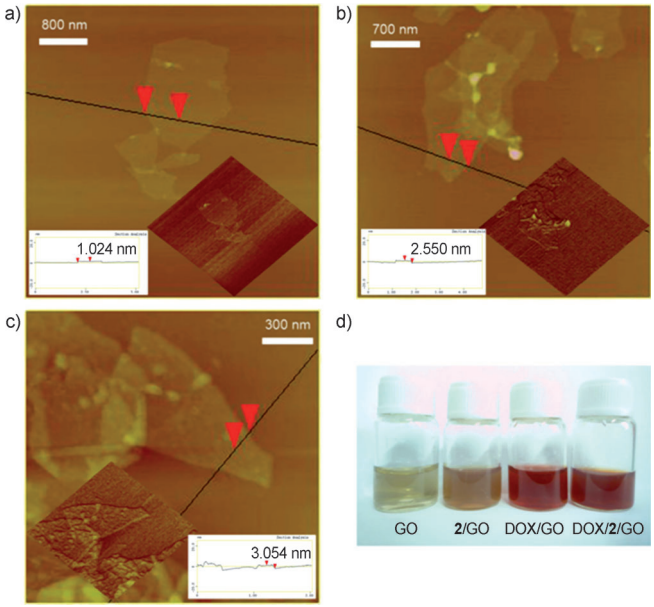

Figure 6. AFM images of a) GO, b) **2**/GO, c) DOX/GO, and d) photographs of GO, **2**/GO, DOX/GO, and DOX/**2**/GO.

DOX/GO, the cross-section analysis showed that the height of the DOX/GO assembly was 3.1 nm (Figure 6c), which indicates attachment of DOX molecules on both sides of the GO sheets. In sharp contrast, the AFM images of the DOX/**2**/GO assembly reveal a height of 4.2 nm (Figure 5b), which is approximately equal to the sum of the height of monolayer GO, the π–π stacking distance, and the height of DOX and **2** attached to both sides of GO sheets mainly as monomers. Moreover, the quantities of uniform distribution protuberances of DOX/**2**/GO indicated that a large amount of DOX and porphyrin were loaded onto GO. Additionally, it is worth noting that this successful loading process showed characteristic color changes that could be readily distinguished by the naked eye (Figure 6d).

Photodynamic effects in vitro: Considering the good photodynamic properties of both GO and porphyrin, we investigated the DNA cleavage ability of **2**/GO and **1**/**2**/GO systems under visible-light irradiation. The agarose gel electrophoresis assay of plasmid DNA is illustrated in Figure 7. In the absence of light, neither **2**/GO nor **1**/**2**/GO displayed any DNA cleavage ability. However, GO showed an ability to cleave DNA with an efficiency of 69% under visible-light irradiation (Figure 7, line 1). The cleavage mechanism of GO may be similar to that of light-activated agents, such as sp^2 carbonaceous nanomaterials,[19] phthalocyanine,[20] and porphyrin derivatives,[21] in which the singlet oxygen ($^1O_2$) species (type II mechanism) is responsible for DNA damage. Significantly, the **2**/GO and **1**/**2**/GO systems exhibited higher DNA photocleavage activity of up to about 80% (Figure 7, lines 2–3) under light irradiation, and most of the closed supercoiled DNA (form I) was cleaved to the nicked circular DNA (form II). The improved DNA cleavage ability could

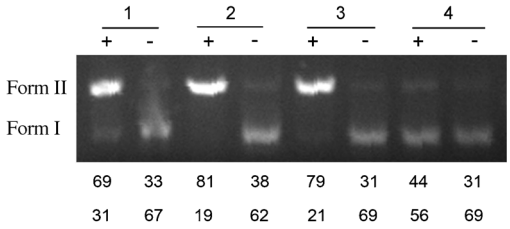

Figure 7. Photocleavage of pMD19-T plasmid DNA (6 ng μL^{-1}) by GO (lane 1, 0.09 mg mL^{-1}), **1**/2/GO (lane 2, [GO] = 0.09 mg mL^{-1}, [**1**] = [**2**] = 63.2 μM, the coverage of **1** in **1**/2/GO was calculated as 54%), and **2**/GO (lane 3, [GO] = 0.09 mg mL^{-1}, [**2**] = 63.2 μM) in the presence (+) and absence (−) of visible light. Lane 4 is the blank control.

be attributed to photoinduced electron transfer from porphyrin to GO, in which the oxygen molecules accept electrons through a charge separation state ($\mathbf{2}^{\bullet+}$/GO$^{\bullet-}$) to generate radical products (type I mechanism),[20] such as superoxide radicals anions ($O_2^{\bullet-}$) and hydroxyl radicals ($^{\bullet}$OH). These highly active radicals are major species that interact with DNA through the free-radical reaction and presumably damage the DNA.

Intracellular uptake in vitro: By taking advantage of the strong hydrophobic interaction between the CD cavity and adamantane moiety, FA-modified β-CD **1** was easily introduced to the DOX/**2**/GO system to improve the biocompatibility and target effect. Consequently, the resulting nanosupramolecular assembly could specifically recognize folate receptor-positive tumor cells owing to the very high affinity between folic acid and folate receptors ($K_d = 10^{-10}$ M).[22] Moreover, it is well-documented that DOX can be released from GO under acidic condition, which is attributed to the increased hydrophilicity and solubility of DOX and reduced hydrogen-bonding interactions between DOX and GO.[8,9] Because the microenvironments of tumor tissues are acidic, this pH-controlled release process is significant in drug-delivery applications.[8] As shown in Figure 8, the anticancer activity tests showed that DOX and **1**/2/DOX/GO displayed similar anticancer activity toward HeLa cell lines, a type of human cervical carcinoma cell widely used as a model for folate receptor-positive cells. In the absence of **1**, the anticancer activity of DOX/**2**/GO decreased by 52% as compared with that of **1**/2/DOX/GO. Moreover, if the folate receptors of the HeLa cells were shielded by excessive FA, the anticancer activity of **1**/2/DOX/GO was also dramatically decreased. These results revealed that FA-modified β-CD **1** plays a very important role in the anticancer effect of the nanosupramolecular assembly. More interestingly, cellular toxicity tests with OCT-1 cell lines (mouse osteoblasts, folate receptor-negative) as model cells showed that the relative cellular viability of **1**/2/DOX/GO reached 97% within 24 h, which was much higher than that of DOX (57%). This result undoubtedly indicates that the **1**/2/DOX/GO nanosupramolecular assembly is almost non-toxic to normal cells over a period of 24 h, as compared with the obvious cellular toxicity of DOX. In addition, the morphology of cancer cells

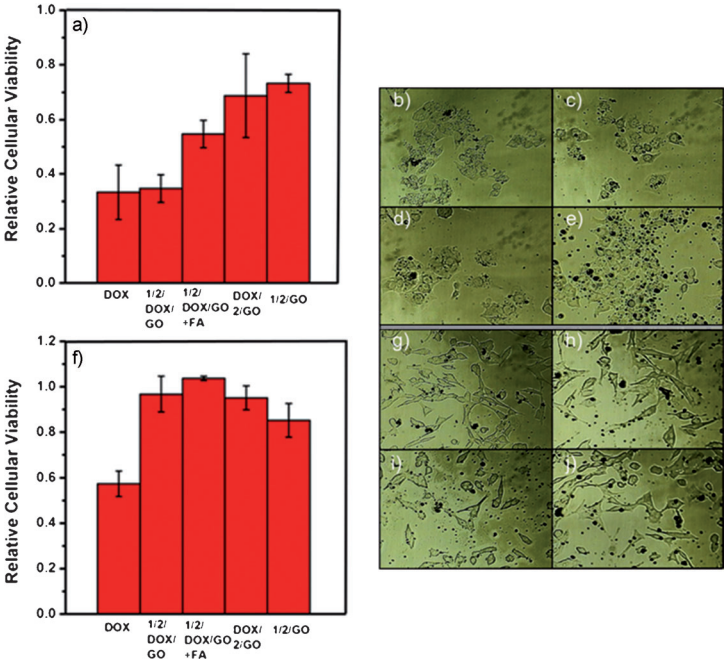

Figure 8. Relative cellular viability of a) HeLa and f) OCT-1 24 h after treatment with DOX, **1**/2/DOX/GO, **1**/2/DOX/GO + excess FA, DOX/**2**/GO, and **1**/2/GO. Photos of Hela cell lines treated with b) blank, c) DOX, d) **1**/2/DOX/GO, e) **1**/2/GO, and OCT-1 cell lines treated with g) blank, h) DOX, i) **1**/2/DOX/GO, j) **1**/2/GO are shown.

and normal cells in the presence of DOX, **1**/2/DOX/GO, and **1**/2/GO showed that DOX and **1**/2/DOX/GO presented similar damage towards cancer cells (Figure 8c, d), but the toxic effect of **1**/2/DOX/GO towards normal cells was much lower than that of DOX (Figure 8h, i). This result is consistent with that of the cell-counting experiment. Therefore, we can deduce that the **1**/2/DOX/GO nanosupramolecular assembly shows no obvious difference in therapeutic effects against cancer cells as compared with DOX, but shows much lower toxicity towards normal cells. A possible explanation may be that the strong affinity between folic acid and the folate receptor facilitates the enrichment of **1**/2/DOX/GO on the surface of cancer cells and thus favors the uptake of the drug into living cells. This process was impeded in OCT-1 cells to a significant extent due to the lack of folate receptors.

Tumor-growth inhibition experiments in vivo: Subsequently, to validate the practical application of **1**/2/DOX/GO in cancer treatment, in vivo anticancer experiments were carried out on a BALB/c nude mice model that contained HeLa cancer cells. As shown in Figure 9, mice with tumors were divided into three groups, one of which was untreated (the control) and two of which were injected with DOX or assembly **1**/2/DOX/GO by the tail vein. The tumor volumes of mice in the untreated group increased steadily over the entire experiment period. Owing to the good anti-tumor effect of doxorubicin, tumor growth was suppressed in the DOX group, with a tumor-growth inhibition of 46% by

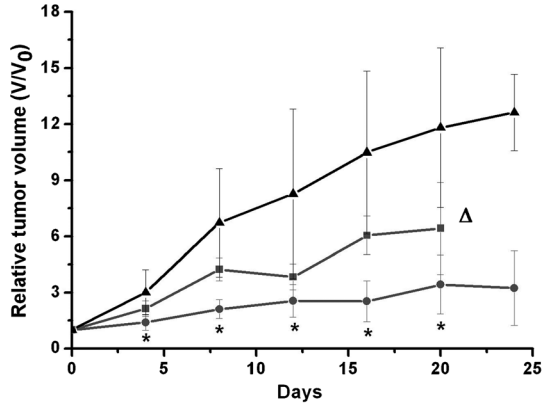

Figure 9. Tumor growth curves for BALB/c nude mice with HeLa cancer cells treated with DOX (■), **1**/**2**/DOX/GO (●), and blank control (▲). The injected dose was normalized to be 1 mg kg^{-1} DOX. Δ = the point at which mice in the DOX group started to die (day 21). The asterisks indicate $P < 0.05$, DOX versus **1**/**2**/DOX/GO, differences are considered statistically significant.

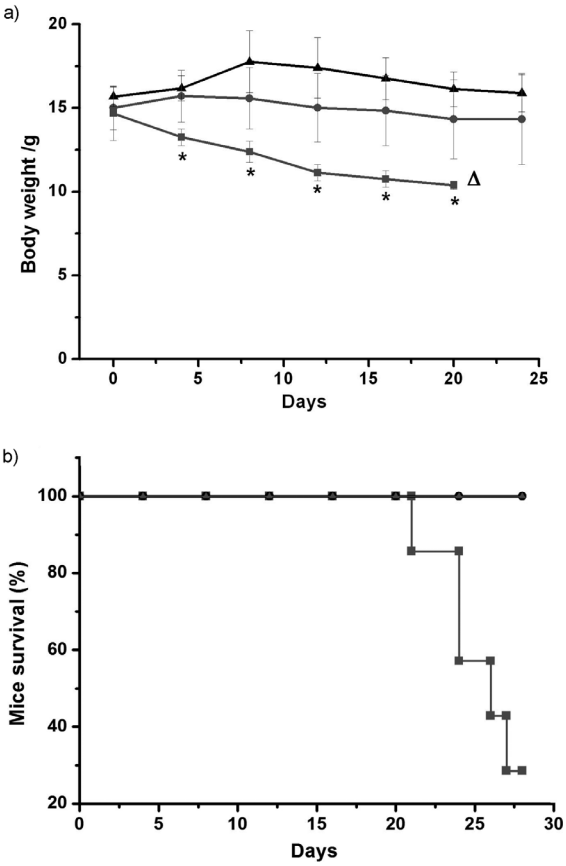

Figure 10. a) Body weight curves for BALB/c nude mice with HeLa cancer cells after treatment with DOX (■), **1**/**2**/DOX/GO (●), and blank control (▲). Δ = the point at which mice in the DOX group started to die (day 21). The asterisks indicate $P < 0.05$, DOX versus **1**/**2**/DOX/GO, and differences are considered statistically significant. b) Survival curves for BALB/c nude mice with HeLa cancer cells after treatment with DOX (■), **1**/**2**/DOX/GO (●), and blank control (▲).

day 20. However, the side-effects of DOX resulted in both loss of body weight and low survival (Figure 10a, b) of mice in later stages of the study because of the high toxicity of DOX toward normal cells and tissues. From day 21 the mice started to die, and less than 30% of the mice survived after day 27.

In sharp contrast, **1**/**2**/DOX/GO showed a much higher tumor-growth inhibition of 71% on day 20. Significantly, compared to DOX alone as drug, no death of the mice could be found even after four weeks. This desired treatment effect might be attributed to the specific binding between the folic acid and the folate receptor expressed on the surface of tumor cells, allowing the assembly **1**/**2**/DOX/GO to accumulate in the malignant tumor issues and to inhibit the growth of the tumor. Because of this targeting effect, the concentration of assembly in the normal tissues might maintain at lower level, thereby reducing side effects (Figure 10a). Moreover, the anti-cancer activity and side-effects of DOX and **1**/**2**/DOX/GO could be distinguished visually from the physical appearance of the mice in terms of tumor size and body weight (Figures S20–S21 in the Supporting Information).

Conclusion

We have constructed a nanosupramolecular assembly by FA-modified β-CD and GO noncovalently linked by an adamantane-grafted porphyrin. The resulting quarternary supramolecular nanoarchitecture benefits from strong π–π stacking between the porphyrin and GO and the high hydrophobic affinity between CD and adamantane, and can be employed as a targeted delivery system to efficiently carry the drug molecules to specific sites with low toxicity to normal cells under physiological conditions. Considering that it is convenient to rationally develop novel modified CDs and expand the use of known CD complexes to recognize other receptor-positive tumors through noncovalent interactions in this modular system, the results shown herein may act as a general protocol for a large library of multifunctional supramolecular biomaterials and could provide a new potential pathway to comprehensively understand the applicability of bioactive nanoscale materials.

Experimental Section

Materials preparation: All chemicals were reagent grade unless noted. β-Cyclodextrin was recrystallized from water twice and dried in vacuo at 90 °C for 24 h before use. 1-Adamantanemethylamine, folic acid, and doxorubicin were purchased from commercial resources and used as received. Mono-6-deoxy-6-ethylenediamino-β-CD[23] (**3**), 5-(4-carboxyphenyl)-10,15,20-triphenylporphyrin[24] (**4**), and graphene oxide[25] were prepared according to procedures reported in the literature. Crude DMSO and DMF were stirred with CaH_2 for 3 d and then distilled under reduced pressure prior to use. Column chromatography was performed on 200–300 mesh silica gel.

Instruments: NMR spectra were recorded by using a Bruker AV400 instrument. UV/Vis spectra were recorded in a conventional quartz cell (light path 10 mm) by using a Shimadzu UV-2401PC spectrophotometer

equipped with a Thermo HAAKE-SC100 temperature controller to keep the temperature at 25 °C. Fluorescence spectra were recorded in a conventional quartz cell (10×10×45 mm) at 25 °C by using an Edinburgh Analytical Instruments FL900CD spectrometer. X-ray photoelectron spectroscopy (XPS) was recorded by using a Kratos Axis Ultra DLD spectrometer equipped with a monochromatic $Al_{K\alpha}$ X-ray source ($h\nu$ = 1486.6 eV), hybrid (magnetic/electrostatic) optics, and a multichannel plate and delay line detector (DLD). For the AFM measurements, a drop of sample suspension was dropped onto newly clipped mica and then air-dried, then examined by using an atomic force microscope (Veeco Company, Multimode, Nano IIIa) in tapping mode in air under ambient conditions. HRTEM (JEOL JEM-2100F) images were obtained at an operating voltage of 200 kV, and the samples were prepared by placing a drop of suspension onto a carbon-coated copper grid. FT-IR spectra were obtained by using a Bio-Rad FTS 6000 Fourier-transform infrared spectrometer. The samples were prepared as tablets by using spectroscopic-grade KBr. The thermogravimetric analysis (TGA) was recorded by using a PTC-10A TG-DTA type instrument with a heating rate of 10 °C min^{-1} from RT to 800 °C.

Mono-6-deoxy-6-(folic acid-γ-ethylenediamino)-β-cyclodextrin (1): 1-Ethyl-3-(3-dimethylaminopropyl)-carbodiimide (EDC; 38.3 mg, 0.2 mmol) and *N*-hydroxysuccinimide (NHS; 23 mg, 0.2 mmol) was added to a solution of folic acid (88.3 mg, 0.2 mmol) in dry DMSO (15 mL) and the mixture was stirred in the absence of light at 30 °C under an N_2 atmosphere for 1 h, then compound **3** (235.4 mg, 0.2 mmol) in dry DMSO (20 mL) was added. The pH of the reaction mixture was adjusted to 9 by adding triethylamine (0.5 mL). The reaction took place in the absence of light at 30 °C under an N_2 atmosphere for 48 h. The mixture was then poured into acetone (500 mL) and the yellow precipitate was filtered. The crude product was purified by column chromatography (silica gel) by using *n*PrOH/H_2O/25% NH_3·H_2O (6:3:1 v/v/v) as the eluent. The product obtained was further purified by MPLC (reversed phase) with a water/ethanol (95:5 v/v) eluent, then compound **1** was obtained as a yellow solid (31% yield). ^{1}H NMR (400 MHz, D_2O, TMS): δ = 1.85–1.88 (m, 2H; H of FA), 2.25 (t, J = 5.8 Hz, 2H; H of FA), 2.69–2.84 (m, 4H; NH-CH_2CH_2-NH), 3.11–3.98 (m, 42H; H of C3, C5, C6, C2, C4 of β-CD), 4.26–4.37 (m, 1H; H of FA), 4.89–5.09 (m, 7H; H of C1 of β-CD), 6.56–6.66 (m, 2H; H of FA), 7.55–7.57 (d, 2H; H of FA), 8.47–8.55 ppm (m, 1H; H of FA); ^{13}C NMR (400 MHz, [D6]DMSO, TMS): δ = 28.5, 32.3, 43.4, 44.8, 46.0, 48.7, 53.7, 60.0, 70.4, 72.1, 72.5, 73.2, 81.6, 83.2, 102.0, 111.4, 122.1, 128.0, 128.7, 148.4, 150.7, 154.8, 156.4, 162.0, 165.6, 172.7, 175.6 ppm; elemental analysis calcd (%) for $C_{63}H_{93}N_9O_{39}$·9H_2O: C 42.93, H 6.35, N 7.15; found: C 42.97, H 6.34, N 7.30; MALDI-TOF MS: *m/z*: 1600.56 $[M+H]^+$, 1622.56 $[M+Na]^+$, 1638.51 $[M+K]^+$.

Adamantane-modified porphyrin (2): 5-(4-Carboxyphenyl)-10,15,20-triphenylporphyrin (**4**; 455.3 mg, 0.69 mmol) and 1-hydroxybenzotrizole (HOBt; 112.1 mg, 0.83 mmol) were dissolved in dry DMF (100 mL) and stirred in an ice-bath for 0.5 h. A solution of 1-adamantanemethylamine (285.6 mg, 1.728 mmol) and *N,N′*-dicyclohexylcarbodiimide (DCC) (171.1 mg, 0.83 mmol) in dry DMF (10 mL) was then added dropwise. The reaction mixture was stirred in the absence of light at 0 °C under an N_2 atmosphere overnight, and then stirred at RT for another 48 h. The mixture was filtered and the filtrate was dried under reduced pressure to remove the solvent. The residue was dissolved in chloroform (100 mL) and washed with water (3×100 mL), then the organic phase was dried over $MgSO_4$. The solvent was removed under reduced pressure and the crude product was washed with hexane and then purified by column chromatography (silica gel; chloroform eluent) to give **2** as a purple solid (47% yield). ^{1}H NMR (400 MHz, $CDCl_3$, TMS): δ = −2.77 (br s, 2H; H of porphyrin), 1.73–1.83 (m, 12H; H of adamantane), 2.09 (s, 3H; H of adamantane), 3.35 (d,, J = 6.3 Hz 2H; CH_2), 6.47 (t, J = 6.8 Hz, 1H; H of C=O-NH), 7.73–7.81 (m, 9H; H of porphyrin), 8.16 (d, J = 8.1 Hz, 2H; H of porphyrin), 8.22 (d, J = 6.1 Hz, 6H; H of porphyrin), 8.31 (d, J = 8.1 Hz, 2H; H of porphyrin), 8.80–8.87 ppm (m, 8H; H of porphyrin); ^{13}C NMR (400 MHz, $CDCl_3$, TMS): δ = 28.4, 34.3, 37.1, 40.6, 51.7, 118.8, 120.5, 120.7, 125.4, 126.9, 127.9, 134.5, 134.68, 134.8, 142.2, 145.6, 168.0 ppm; ESI-MS: *m/z*: 828.37 $[M+Na]^+$; elemental analysis calcd (%) for $C_{56}H_{47}N_5O$: C 83.45, H 5.88, N 8.69; found: C 83.26, H 6.00, N 8.46.

Complex 2/GO: Compound **2** (22.3 mg) was dissolved in DMSO (10 mL) and then added dropwise to an aqueous suspension of GO (0.2 mg mL^{-1}, 50 mL), then deionized water (40 mL) was added. The mixture was stirred for 24 h, then filtered through a 450 nm filter and the residue was dispersed in deionized water (100 mL) by ultrasonication to remove DMSO. Then the suspension was centrifuged at 4000 rpm for 5 min to remove undissolved porphyrin and large pieces of GO. The process was repeated a further nine times to obtain a suspension of **2**/GO; the resulting complex was stored at 4 °C.

Complex DOX/GO: DMSO (10 mL) was added to an aqueous suspension of GO (0.2 mg mL^{-1}, 50 mL), then DOX·HCl (45 mg in 40 mL deionized water) was added, then the pH value of the final mixture was adjusted to 8 by using triethylamine and stirred for 24 h. The mixture was then filtered through a 450 nm filter and the residue was dispersed in deionized water (100 mL) by ultrasonication to remove DMSO and free DOX. The suspension was then centrifuged at 4000 rpm for 5 min to remove large pieces of GO. The process was repeated a further nine times to give a suspension of DOX/GO; the resulting complex was stored at 4 °C.

Complex DOX/2/GO: Compound **2** (22.3 mg) was dissolved in DMSO (10 mL) and then added dropwise to an aqueous suspension of GO (0.2 mg mL^{-1}, 50 mL). DOX·HCl (45 mg) in deionized water (40 mL) was added, then the pH value was adjusted to 8 by using triethylamine and the final mixture was stirred for 24 h. The mixture was filtered through a 450 nm filter and the residue was dispersed in deionized water (100 mL) by ultrasonication to remove DMSO and free DOX. Then the suspension was centrifuged at 4000 rpm for 5 min to remove undissolved porphyrin and large pieces of GO. The process was repeated a further nine times to give a suspension of **2**/DOX/GO; the resulting complex was stored at 4 °C.

Cytotoxicity experiments: Human cervical carcinoma (HeLa) cells and OCT-1 mouse osteoblasts were cultured in Dulbecco's modified Eagle's medium (DMEM) supplemented with 10% fetal bovine serum (FBS) and gentamicin (80 μg mL^{-1}) in 24-well plates (2×10^4 cells mL^{-1}, 1 mL per well) for 24 h. The cells were incubated with DOX, **1**/**2**/DOX/GO, **1**/**2**/DOX/GO + FA, DOX/**2**/GO, and **1**/**2**/GO ([DOX] = 3 μM, [**1**] and [**2**] = 2 μM in each sample) for 4 h. Then all the cells were transferred into fresh cell medium. After incubation for a further 24 and 48 h, the relative cellular viability was measured by using a cell-count assay.

Animal model experiment: All experimental procedures were approved and in accordance with China's National Code of Animal Care for Scientific Experimentation. The experiment was also assessed by the Animal Experimentation Ethics Committee of Nankai University. Four-week-old female BALB/c nude mice (n = 21) were fed with folic acid-deficient chow during the whole experiment period. The HeLa tumor models were generated by subcutaneous injection of 5×10^6 HeLa cells in DMEM (100 μL) into the left groin of each mouse. When the tumor volume reached 50–100 mm^3 (ca. 13 days after tumor implantation), the mice were divided into three groups (seven mice per group). Two of the groups of mice were injected with 200 μL of DOX or **1**/**2**/DOX/GO through the tail vein every four days. The doses were set at 1 mg kg^{-1} DOX. The tumor volumes (V) were measured by using a caliper every 4 d and calculated by using the following formula: $V = 0.5\times$(tumor length)$\times$(tumor width)^2. The relative tumor volumes were calculated as V/V_0 (V_0 is the tumor volume when drug injection began).

Statistical analysis of the data was carried out by using Student's t-test. Differences were considered statistically significant if the P value was < 0.05.

Acknowledgements

We thank the 973 Program (2011CB932502), the NNSFC (20932004, 91027007) and the Program for New Century Excellent Talents in University (NCET-10-0500) for financial support.

[1] a) M. A. Mintzer, E. E. Simanek, *Chem. Rev.* **2009**, *109*, 259–302; b) S. Lee, H. Chen, T. V. O'Halloran, S. T. Nguyen, *J. Am. Chem. Soc.* **2009**, *131*, 9311–9320.

[2] a) K. J. Landmark, S. DiMaggio, J. Ward, C. Kelly, S. Vogt, S. Hong, A. Kotlyar, A. Myc, T. P. Thomas, J. E. Penner-Hahn, J. R. Baker, Jr., M. M. B. Holl, B. J. Orr, *ACS Nano* **2008**, *2*, 773–783; b) K. Hayashi, K. Ono, H. Suzuki, M. Sawada, M. Moriya, W. Sakamoto, T. Yogo, *ACS Appl. Mater. Interfaces* **2010**, *2*, 1903–1911; c) J. Zhang, M. Riskin, R. Freeman, R. Tel-Vered, D. Balogh, H. Tian, I. Willner, *ACS Nano* **2011**, *5*, 5936–5944.

[3] a) J.-Z. Du, T.-M. Sun, W.-J. Song, J. Wu, J. Wang, *Angew. Chem.* **2010**, *122*, 3703–3708; *Angew. Chem. Int. Ed.* **2010**, *49*, 3621–3626; b) K. S. Soppimath, L.-H. Liu, W. Y. Seow, S.-Q. Liu, R. Powell, P. Chan, Y. Y. Yang, *Adv. Funct. Mater.* **2007**, *17*, 355–362; c) H. H. Dam, F. Caruso, *Adv. Mater.* **2011**, *23*, 3026–3029.

[4] a) Z. Liu, X. Sun, N. Nakayama-Ratchford, H. Dai, *ACS Nano* **2007**, *1*, 50–56; b) Z. Liu, J. T. Robinson, X. Sun, H. Dai, *J. Am. Chem. Soc.* **2008**, *130*, 10876–10877; c) S. Dhar, Z. Liu, J. Thomale, H. Dai, S. J. Lippard, *J. Am. Chem. Soc.* **2008**, *130*, 11467–11476.

[5] a) D. Peer, J. M. Karp, S. Hong, O. C. FaroKhzad, R. Margalit, R. Langer, *Nat. Nanotechnol.* **2007**, *2*, 751–760; b) K. J. Cho, X. Wang, S. M. Nie, Z. Chen, D. M. Shin, *Clin. Cancer Res.* **2008**, *14*, 1310–1316; c) X. W. Dong, R. J. Mumper, *Nanomedicine* **2010**, *5*, 597–615.

[6] K. S. Novoselov, A. K. Geim, S. V. Morozov, D. Jiang, Y. Zhang, S. V. Dubonos, I. V. Grigorieva, A. A. Firsov, *Science* **2004**, *306*, 666–669.

[7] a) Z. Liu, W. B. Cai, L. N. He, N. Nakayama, K. Chen, X. M. Sun, X. Y. Chen, H. J. Dai, *Nat. Nanotechnol.* **2007**, *2*, 47–52; b) Z. Liu, C. Davis, W. Cai, L. He, X. Chen, H. Dai, *Proc. Natl. Acad. Sci. USA* **2008**, *105*, 1410–1415; c) P. Cherukuri, C. J. Gannon, T. K. Leeuw, H. K. Schmidt, R. E. Smalley, S. A. Curley, R. B. Weisman, *Proc. Natl. Acad. Sci. USA* **2006**, *103*, 18882–18886.

[8] X. Sun, Z. Liu, K. Welsher, J. T. Robinson, A. Goodwin, S. Zaric, H. Dai, *Nano Res.* **2008**, *1*, 203–212.

[9] L. Zhang, J. Xia, Q. Zhao, L. Liu, Z. Zhang, *Small* **2010**, *6*, 537–544.

[10] M. R. Eftink, M. L. Andy, K. Bystrom, H. D. Perlmutter, D. S. Kristol, *J. Am. Chem. Soc.* **1989**, *111*, 6765–6772.

[11] H. Wang, K. Liu, K.-J. Chen, Y. Lu, S. Wang, W.-Y. Lin, F. Guo, K. Kamei, Y.-C. Chen, M. Ohashi, M. Wang, M. A. Garcia, X.-Z. Zhao, C. K.-F. Shen, H.-R. Tseng, *ACS Nano* **2010**, *4*, 6235–6243.

[12] a) Y. Xu, L. Zhao, H. Bai, W. Hong, C. Li, G. Shi, *J. Am. Chem. Soc.* **2009**, *131*, 13490–13497; b) A. Wojcik, P. V. Kamat, *ACS Nano* **2010**, *4*, 6697–6706.

[13] X. Yang, X. Zhang, Z. Liu, Y. Ma, Y. Huang, Y. Chen, *J. Phys. Chem. C* **2008**, *112*, 17554–17558.

[14] C. Hontoria-Lucas, A. J. Lopez-Peinado, J. D. Lopez-Gonzalez, M. L. Rojas-Cervantes, R. M. Martin-Aranda, *Carbon* **1995**, *33*, 1585–1592.

[15] a) S. Stankovich, D. A. Dikin, R. D. Piner, K. A. Kohlhaas, A. Kleinhammes, Y. Jia, Y. Wu, S. B. T. Nguyen, R. S. Ruoff, *Carbon* **2007**, *45*, 1558–1565; b) C. Mattevi, G. Eda, S. Agnoli, S. Miller, K. A. Mkhoyan, O. Celik, D. Mastrogiovanni, G. Granozzi, E. Garfunkel, M. Chhowalla, *Adv. Funct. Mater.* **2009**, *19*, 2577–2583; c) A. Bagri, C. Mattevi, M. Acik, Y. J. Chabal, M. Chhowalla, V. B. Shenoy, *Nat. Chem.* **2010**, *2*, 581–587.

[16] O. Akhavan, *Carbon* **2010**, *48*, 509–519.

[17] Y. Gao, H.-L. Yip, K.-S. Chen, K. M. O'Malley, O. Acton, Y. Sun, G. Ting, H. Chen, A. K.-Y. Jen, *Adv. Mater.* **2011**, *23*, 1903–1908.

[18] a) M. M. T. Khan, S. Srivastava, *Polyhedron* **1988**, *7*, 1063–1068; b) H. S. O. Chan, T. S. A. Hor, M. M. Sim, K. L. Tan, B. T. G. Tan, *Polym. J.* **1990**, *22*, 883–892; c) K. C. Dash, B. Folkesson, R. Larsson, M. Mohapatra, *J. Electron Spectrosc. Relat. Phenom.* **1989**, *49*, 343–357.

[19] N. Gandra, P. L. Chiu, W. Li, Y. R. Anderson, S. Mitra, H. He, R. Gao, *J. Phys. Chem. C* **2009**, *113*, 5182–5185.

[20] M. Zhang, T. Murakami, K. Ajima, K. Tsuchida, A. S. D. Sandanayaka, O. Ito, S. Iijima, M. Yudasaka, *Proc. Natl. Acad. Sci. USA* **2008**, *105*, 14773–14778.

[21] M. Ethirajan, Y. Chen, P. Joshi, R. K. Pandey, *Chem. Soc. Rev.* **2011**, *40*, 340–362.

[22] P. S. Low, W. A. Henne, D. D. Doorneweerd, *Acc. Chem. Res.* **2008**, *41*, 120–129.

[23] B. L. May, S. D. Kean, C. J. Easton, S. F. Lincoln, *J. Chem. Soc. Perkin Trans. 1* **1997**, 3157–3160.

[24] M. Y. Jiang, D. Dolphin, *J. Am. Chem. Soc.* **2008**, *130*, 4236–4237.

[25] a) W. S. Hummers, Jr., R. E. Dffeman, *J. Am. Chem. Soc.* **1958**, *80*, 1339; b) M. Hirata, T. Gotou, S. Horiuchi, M. Fujiwara, M. Ohba, *Carbon* **2004**, *42*, 2929–2937.

Received: November 2, 2011
Published online: February 28, 2012

